Journal of Chromatography A, 1217 (2010) 1485–1495

Contents lists available at ScienceDirect

Journal of Chromatography A

journal homepage: www.elsevier.com/locate/chroma

Performance of new prototype packed columns for very high pressure liquid chromatography

Fabrice Gritti, Georges Guiochon*

Department of Chemistry, University of Tennessee, Knoxville, TN 37996-1600, USA

ARTICLE INFO

Article history:
Received 8 September 2009
Received in revised form
14 December 2009
Accepted 23 December 2009
Available online 4 January 2010

Keywords:
Very high pressure liquid chromatography
Heat effects
Temperature gradients
BEH-C_{18} columns
Column efficiency
Naphtho[2,3-a]pyrene
Acetonitrile mobile phase

ABSTRACT

The reduced heights equivalent to a theoretical plate (HETP) of naphtho[2,3-a]pyrene were measured at room temperature on two sets of new prototype columns designed to be used in very high pressure liquid chromatography (VHPLC). The mobile phase used was pure acetonitrile. The columns are 50, 100, and 150 mm long. Those of the first set are 2.1 mm I.D., those of the second set, 3.0 mm I.D. The performance of these new columns were compared to those of the first generation of VHPLC columns, commercially available in 2.1 mm I.D. The prototype and commercial columns behave similarly at low reduced linear velocities ($\nu < 5$), when the heat effects are negligible. At high flow rates, the shorter prototype columns have a twice better efficiency and less steep C-branches than the commercial columns. In contrast, the C-branch of the 150 mm long prototype columns are slightly steeper than those of the commercial columns. The important contribution to the reduced HETP that is due to the heat effects at high flow rates can in part be accounted for by a band broadening model governed by a flow mechanism with the shortest prototype columns. The sole heat effects cannot, however, explain the mediocre reduced HETPs of the 2.1 and 3.0 I.D. 150 mm long prototype columns. It seems that radial heterogeneity of the flow rate of the long prototype columns is significantly larger than that of the short columns. The contribution of the packing heterogeneity adds up to that of the heat effects to yield a poor column efficiency when sub-2μm are packed into thin, long column tubes.

1. Introduction

Very high pressure liquid chromatography (VHPLC) allows fast and highly efficient separations [1]. At their optimum velocity, the first generation of VHPLC columns (Acquity UPLC BEH-C_{18}) provide plate counts of the order of 325,000 plates per meter, slightly larger than the 250,000 plates per meter that the 2.7 μm fused core particles can yield [2]. The column impedance, E_{min} [3], combines the minimum plate height, H_{min}, the column permeability, k_0, and the total porosity of the packed bed, with $E_{min} = (H^2_{min}/k_0)\epsilon_t$. Columns packed with fused core particles surpass VHPLC particles by a factor 1.7 (1100 *versus* 1900). The minimum impedance of commercial monolithic columns with through-pore size of 3.5 μm is smaller, due to their exceptionally high permeability, equivalent to that of a column packed with 11 μm particles ($E_{min} = 400$) [4]. But monolithic columns can only deliver a maximum plate count of ca. 125, 000 m^{-1}, which is insufficient to achieve a satisfactory peak resolution of complex mixtures in 1D and/or even in 2D liquid chromatography.

Columns for VHPLC are packed with sub-2 μm spherical particles; their permeability is necessarily low while their optimum velocity for maximum column efficiency is high. So, they must routinely be run at inlet pressures as high as 1 kbar in order to benefit from their exceptionally low plate heights (ca. 3 μm) and to perform fast separations. Under such high pressure gradients along the column and with such high linear flow velocities, the frictional heating of the eluent percolating the interparticle volume [5–7] causes the formation of longitudinal and radial temperature gradients [8]. The consequences of the thermal heterogeneity of the packed bed on its chromatographic properties are (1) a decrease of the analyte retention factor due to the increase of the average column temperature from its entrance to its outlet (longitudinal temperature gradients [9,10]); and (2) a decrease of the column efficiency as a result of the radial temperature gradients (from the center to the wall of the column), which causes a radial viscosity, hence velocity profile. The sample migration velocity across the column contributes to broaden eluted peaks. In order to account for the dispersive contribution of these effects, an additional HETP term due to these heat effects must be added to the classical isothermal van Deemter plots [11,12].

This additional HETP term can be estimated based on the general dispersion theory of Aris in cylindrical tubes [13,14]. The conditions of validity of the Aris' dispersion model are approximately satisfied

* Corresponding author. Tel.: +1 865 974 0733; fax: +1 865 974 2667.
E-mail addresses: guiochon@utk.edu, guiochon@ion.chem.utk.edu (G. Guiochon).

0021-9673/$ – see front matter © 2009 Elsevier B.V. All rights reserved.
doi:10.1016/j.chroma.2009.12.057

Table 1
Physico-chemical properties of the new prototype columns given by the manufacturer and measured in our lab.[a,b]

Neat silica	Bridged ethylsiloxane/silica hybrid (BEH)		
Particle size (μm)	1.7		
Pore diameter (Å)	130		
Surface area (m^2/g)	185		
Bonded phase analysis	BEH-C_{18}		
Total carbon (%)	18		
Surface coverage (μmol/m^2)	3.10		
Endcapping	Proprietary		
Packed columns analysis	Set 1: small inner diameter		
Serial number	01672902020A01	01672834020A01	0.167201420A01
Dimension (mm × mm)	2.1 × 50	2.1 × 100	2.1 × 150
Total porosity[a]	0.658 ± 0.003	0.655 ± 0.003	0.655 ± 0.003
External porosity[b]	0.370 ± 0.005	0.377 ± 0.005	0.385 ± 0.005
Particle porosity	0.46 ± 0.02	0.45 ± 0.02	0.44 ± 0.02
Kozeny-Carman constant K_c	143.8	139.3	140.5
Packed columns analysis	Set 2: large inner diameter		
Serial number	01672902130F02	01672902130F03	01672902130F04
Dimension (mm × mm)	3.0 × 50	3.0 × 100	3.0 × 150
Total porosity[a]	0.643 ± 0.003	0.654 ± 0.003	0.655 ± 0.003
External porosity[b]	0.368 ± 0.005	0.381 ± 0.005	0.383 ± 0.005
Particle porosity	0.43 ± 0.02	0.44 ± 0.02	0.44 ± 0.02
Kozeny-Carman constant K_c	152.8	150.7	149.9

[a] Measured by pycnometry (THF-CH_2Cl_2).
[b] Measured by inverse size exclusion chromatography (polystyrene standards).

for long columns and strongly retained samples, for which the residence time of analytes are longest [14]. This additional HETP term is proportional to the average migration velocity of the sample, to the square of the temperature difference between the center and the wall region of the column, to the square of the column diameter and is inversely proportional to the radial dispersion coefficient. The obvious strategy to minimize heat effects is to decrease as much as possible the amplitude of the radial temperature gradients by keeping the column under near adiabatic conditions (e.g., in the air-oven compartment of the instrument), which essentially results into the formation of a longitudinal temperature gradient [15]. Experimental subterfuges such as injecting an eluent cooler than the oven temperature can improve column performance to a point where it does not deviate much from that of an isothermal column [15]. In the entrance region of the column, the analyte migrates slower in the central than in the wall region of the tube while the opposite is true beyond a critical column length. The velocity compensation between the first and second portion of the column allows the band profile, initially warped in one direction, to reform into a radially flat one that corresponds to near piston flow before the band exits the column. The undesirable thermal effects are minimized but the determination of the optimal temperature of the air-oven and the inlet eluent is empirical and requires a long trial and error process. A practical strategy consists in increasing the column temperature because the eluent viscosity decreases, the smaller pressure drop causes a lesser frictional heating and the molecular diffusivity increases. Several short VHPLC columns can then be coupled in series to produce very high efficiencies [16]. Another approach consists in limiting the heat loss through the column wall by coating the inner wall of the stainless steel tube with an insulating material (e.g., silica, ceramic).

In this work, we report on the performance of new prototype columns developed for applications in VHPLC. These columns were packed with particles of a new packing material for which no information, including no physico-chemical properties and no particle characteristics have yet been released. These columns are the forerunners of the second generation of VHPLC columns (phase II Acquity UPLC manufacturing process) and were recently presented at Pittcon2009 [17]. We used six columns of different sizes, three columns have an inner diameter of 2.1 mm and lengths of 50, 100, and 150 mm; the other three columns have the same lengths but an inner diameter of 3.0 mm. We measured the efficiencies of these columns at 294 K, using pure acetonitrile as the eluent and naphtho[2,3-a]pyrene as the analyte [18,12,15] and we studied their mass transfer properties. The performance of these new columns is compared to that of the conventional VHPLC columns which were studied under the same experimental conditions (eluent, analyte, temperature, column size, and instrument) [15]. Finally, we discuss the influence of the length and inner diameter of the new prototype columns on their mass transfer behavior at high linear velocity, when heat effects are significant.

2. Experimental

2.1. Chemicals

The mobile phase used in this work was pure acetonitrile. Dichloromethane and tetrahydrofuran were also used in smaller amounts to measure the column hold-up volume by pycnometry. These three solvents were HPLC grade from Fisher Scientific (Fair Lawn, NJ, USA). The mobile phase was filtered before use on a surfactant-free cellulose acetate filter membrane, 0.2 μm pore size (Suwannee, GA, USA). Naphtho[2,3-a]pyrene was used as the probe analyte. It was obtained from Aldrich (Milwaukee, WI, USA). Ten polystyrene standards (MW = 590, 1100, 3680, 6400, 13,200, 31,600, 90,000, 171,000, 560,900, and 900,000) were used to acquire inverse size exclusion chromatography data (ISEC). They were purchased from Phenomenex (Torrance, CA, USA).

2.2. Columns

The six (50 mm × 2.1 mm, 100 mm × 2.1 mm, 150 mm × 2.1 mm, 50 mm × 3.0 mm, 100 mm × 3.0 mm, and 150 mm × 3.0 mm) new prototype BEH-C_{18} columns used were a gift from the column manufacturer (Waters, Milford, MA, USA). The synthesis of the silica matrix is based on the organic (ethyl)/inorganic

(silica) hybrid technology. The main characteristics of the bare porous silica and those of the final derivatized packing material are summarized in Table 1.

The columns were kept horizontal in direct contact with the laboratory atmosphere, in the air-oven of the instrument (see next section), protected from air drafts and of temperature perturbations. The column tube dissipates heat only by natural convection and radiation. The surface temperature of the external wall of the stainless steel tube was measured using a series of surface thermocouples. All relevant information regarding the measurement method and the materials used is given elsewhere [19]. The precision of the thermocouples is ±0.2 K. The local temperatures were measured at four, nine, and nine different axial positions on the 50, 100, and 150 mm long columns, respectively.

2.3. Apparatus

The apparatus used was an Acquity UPLC liquid chromatograph (Waters, Milford, MA, USA). This instrument includes a quaternary solvent delivery system, an auto-sampler with a 1 μL sample loop, a monochromatic UV detector, a column oven, and a data station running the Empower data software from Waters. From the exit of the Rheodyne injection valve to the column inlet and from the column outlet to the detector cell, the total extra-column volume of the instrument is 14.3 μL, measured as the apparent hold-up volume of a zero-volume union connector in place of the column. A time offset of 0.66 s was measured after the zero injection time was recorded. The first and second moment were all corrected from these extra-column volume contributions. The flow rate delivered by the high pressure pumps of the instrument is true at the column inlet. During the HETP measurements, the inlet flow rate was successively fixed at 0.03, 0.06, 0.12, 0.20, 0.30, 0.40, 0.50, 0.60, 0.70, 0.85, 1.00, 1.15, 1.30, 1.45, 1.60, 1.75, and 1.90 mL/min when possible. Up to 1.00 mL/min, the maximum pressure allowed during a run was 1034 bar. Above 1.00 mL/min, it decreased to 972, 910, 848, 785, 723, and 661 bar at 1.15, 1.30, 1.45, 1.60, 1.75, and 1.90 mL/min, respectively.

The laboratory temperature was controlled at 294 ± 1 K by the lab air conditioning system.

3. Results and discussion

We first discuss some important characteristics of the columns, including their external porosities and their permeability. Then, we report on the HETP plots of these new prototype columns, on the parameters of these curves and compare their performance to those of VHPLC columns of the first generation. We discuss the influence of the column diameter on its performance and the role played by the friction heat effect in the mass transfer mechanism at high linear velocities. Finally, we discuss whether a diffusive dispersion model (based on the Aris dispersion theory) or a flow dispersion model is more appropriate to account for the large *C*-value observed in the van Deemter equation.

3.1. Permeability of the new prototype columns

The external porosity, ϵ_e, of packed beds is an important characteristic of HPLC columns because it affects the column permeability, which is essentially controlled by the average particle size, d_p. The shape of the packed particles, their size distribution, and the chemical nature of their external surface play also a significant role in the column permeability but their impact is more difficult to assess. Their effect is empirically lumped into the Kozeny-Carman constant, K_c. The permeability k_0 of the packed column writes:

$$k_0 = \frac{K_c(1-\epsilon_e)^2}{d_p^2 \epsilon_e^3} \quad (1)$$

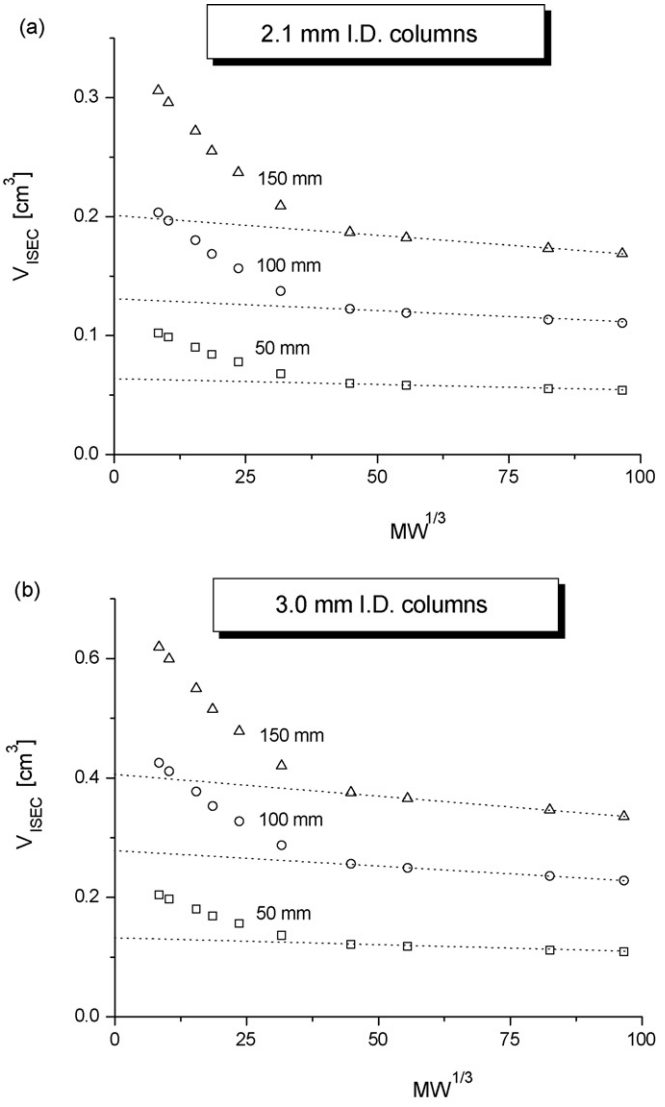

Fig. 1. ISEC measurements. Eluent: pure tetrahydrofuran. Flow rate: 0.20 mL/min. Plots of the elution volume of 10 polystyrene standards *versus* the cubic root of their known average molecular weights ($MW^{1/3}$). Six new prototypes VHPLC columns were studied. (A) 2.1 mm column I.D. (B) 3.0 mm I.D. The external porosities, ϵ_e, were extrapolated at $MW = 0$ from the excluded ISEC branch of each plot (dotted lines).

The external porosities were derived from ISEC experiments. Fig. 1A and B represents the ISEC plots of the two sets of prototype columns (2.1 and 3.0 mm I.D.), as the elution volume of the polystyrene standards corrected for the extra-column contributions, V_{ISEC}, *versus* the cubic root of their molecular weight, $MW^{1/3}$. This representation is convenient because $MW^{1/3}$ is proportional to the hydrodynamic diameter of the random coil formed by the polymer molecules [20]. When the size of the polymer coil is much smaller than the particle diameter (1.7 μm), the exclusion volume of the polymer decreases almost linearly with increasing molecular size. This is the case for polystyrene standards with molecular weights of 171,000 (D_h = 245 Å), 560,900 (D_h = 479 Å), and 900,000 (D_h = 625 Å), which are all excluded from the pore network of the new prototype material. The external porosities are measured from the linear extrapolation of this excluded ISEC branch to $MW = 0$ (e.g. when the size of the

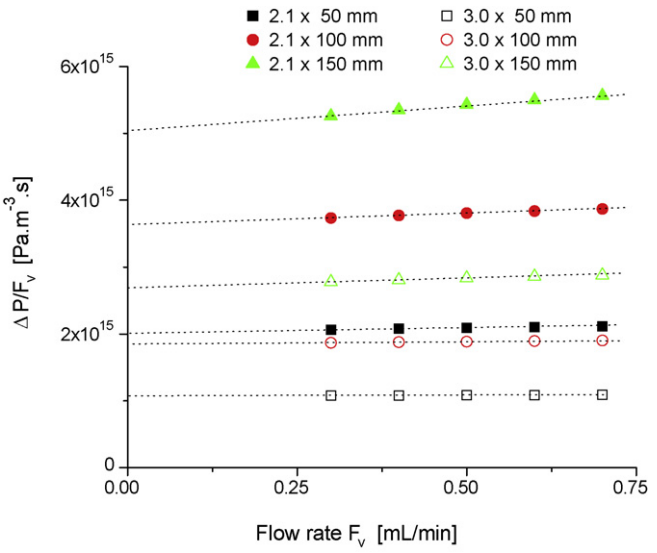

Fig. 2. Permeability data. Permeating liquid: pure acetonitrile, viscosity taken at T = 294 K and $P = P^0$: 0.36 cP. Flow rate range: 0.30–0.70 mL/min. Six new prototypes VHPLC columns were studied as indicated in the legend of the graph. Plots of the ratio of the pressure drop, ΔP (corrected for the extra-column pressure drop) to the column inlet flow rate, F_v. The permeability of the columns were determined from the extrapolation of their respective plots at a zero flow rate.

polymer coil tends toward zero). The values are listed in Table 1. We observe that the longer the column, the less densely packed are the particles. For both sets of columns, the external porosity increases from 0.370 to 0.385 when the column length increases from 50 to 150 mm. This is consistent with the columns being packed by the slurry process. The longer columns are not as densely packed as the shorter columns, due to their larger hydraulic resistance during the packing process. In contrast, the column diameter seems to have no effect on the external porosities, given the relative precision of the ISEC experiments.

The external porosities of the first generation of VHPLC columns (2.1 mm I.D.) were very comparable to those measured in this work. They increased from 0.373 to 0.380 when their length increased from 50 to 150 mm [8,10].

The Kozeny-Carman constants, K_c, were determined by measuring the column pressure drops using pure acetonitrile as the eluent. The viscosity of acetonitrile, η_S, at 294 K is 0.36 cP [21]. The Kozeny-Carman constant is given by

$$K_c = \frac{d_p^2 \epsilon_e^3 \pi R_c^2}{\eta_S (1-\epsilon_e)^2 L} \frac{\Delta P}{F_v} \quad (2)$$

where R_c is the inner tube radius, L the column length, ΔP the column pressure drop corrected for the extra-column pressure drop contributions (caused by the column stabilizer before the column entrance and the capillary restrictor downstream the column), and F_v the column inlet flow rate. The inlet column pressure was measured at different inlet flow rates from 0.30 to 0.70 mL/min. The ratios $(\Delta P/F_v)$ for each column are plotted in Fig. 2*versus* the flow rate. This ratio increases slightly with increasing flow rate because the viscosity of acetonitrile increases with the pressure. The variation of the viscosity of acetonitrile with the local temperature, T, and pressure, P, is [8]:

$$\eta_S(T,P) = 10^{\left(A_\eta + \frac{B_\eta}{T}\right)} (1 + \zeta[P-1]) \quad (3)$$

where $A_\eta = -1.757$, $B_\eta = 386$ K, and $\zeta = 6.263 \times 10^{-4}$ bar^{-1}. Equation 3 explains why the slope of the plots in Fig. 2 increases with increasing column length or decreasing column diameter. The maximum average column pressure at a flow rate of 0.70 mL/min is equal to 325 bar (column with 2.1 mm I.D. and 150 mm length). The average viscosity of acetonitrile is then 0.43 cP, 12% larger than the viscosity measured under atmospheric pressure at 294 K. This result agrees with the experimental increase of the ratio $(\Delta P/F_v)$ seen in Fig. 2 (+10%) between the extrapolated flow rate, $F_v = 0$, and 0.70 mL/min. Heat effects remain small in this flow rate range and most likely explain the smaller experimental difference.

Therefore, the permeability of the column can be measured precisely by extrapolating linearly the value of $(\Delta P/F_v)$ to a zero flow rate. The Kozeny-Carman constant is then derived according to Eq. (2). The values obtained for all the columns are listed in Table 1. The average Kozeny-Carman constants of the 2.1 and 3.0 mm I.D. columns are approximately 140 and 150, respectively. These values are not significantly different from those previously measured on the first generation of VHPLC columns (K_c = 140 for 2.1 mm I.D. columns).

In conclusion, the columns of the new generation of VHPLC columns have external porosities and Kozeny-Carman constants similar to those of the first generation, produced in phase I of the manufacturing process.

3.2. Comparison between the efficiencies of the first and second generation of VHPLC columns

The reduced HETPs of naphtho[2,3-a]pyrene were measured on the six new prototype columns. The flow rate of pure acetonitrile was increased from 0.03 to either 1.90 mL/min or to the highest flow rate allowed by the maximum pressure limit of the Acquity instrument and the Empower data station during a run. It should be emphasized that the HETP concept is valid only for isothermal and isobaric columns. At high velocities, it applies only locally at the axial coordinate z of VHPLC columns. The apparent experimental HETP was calculated from the following equation:

$$H = \frac{\Sigma H(z)\Delta z}{L} = L \frac{\left(t^r_{1/2} - t^f_{1/2}\right)^2 - \left(t^r_{1/2,e} - t^f_{1/2,e}\right)^2}{5.545(t_R - t_e)^2} \quad (4)$$

where t_R and t_e are the retention times recorded for the peak apices of the probe compound with and without a column fitted on the instrument, $t^r_{1/2}$ and $t^r_{1/2,e}$, and $t^f_{1/2}$ and $t^f_{1/2,e}$ are the rear and the front widths of the peak measured at half-height of the peak. Note that, in this work, we measured apparent reduced plate heights in the sense that, in very high pressure liquid chromatography, the eluent density and viscosity vary along the column while its pressure decreases by about 1000 bar and the temperature increases by about 20 K under the extreme conditions of high flow rate, from column inlet to outlet. This leads to variations of the local flow rate and HETP, as discussed thoroughly in [11]. The main point of this work, however, is that we compare similar columns operated under the same set of experimental conditions, on the basis of the h data recorded for them.

The results are gathered in Fig. 3A for the second generation of VHPLC columns. By convention the reduced linear velocity was calculated from the interstitial linear velocity at the column inlet $(u_{e,inlet} = (F_v/\epsilon_e \pi R^2))$ and the molecular diffusion coefficient of naphtho[2,3-a]pyrene was estimated from the Wilke and Chang equation [22] at 294 K and under atmospheric pressure $(D_m(294\,\text{K}, P^0) = 1.22 \times 10^{-5}\,\text{cm}^2/\text{s})$. The average particle size was determined from the Coulter counter method at 1.7 μm, according to the manufacturer. Fig. 3B shows the same HETP plots but with the first generation of VHPLC columns (2.1 mm I.D.) measured under the very same conditions.

The diffusion branches of the curves in Fig. 3A and B are nearly superimposed for the two generations of columns, meaning that the B-term of both column types is exactly the same. This certainly means that the chemical and physico-chemical properties of the packing material have not been changed from the first to the second

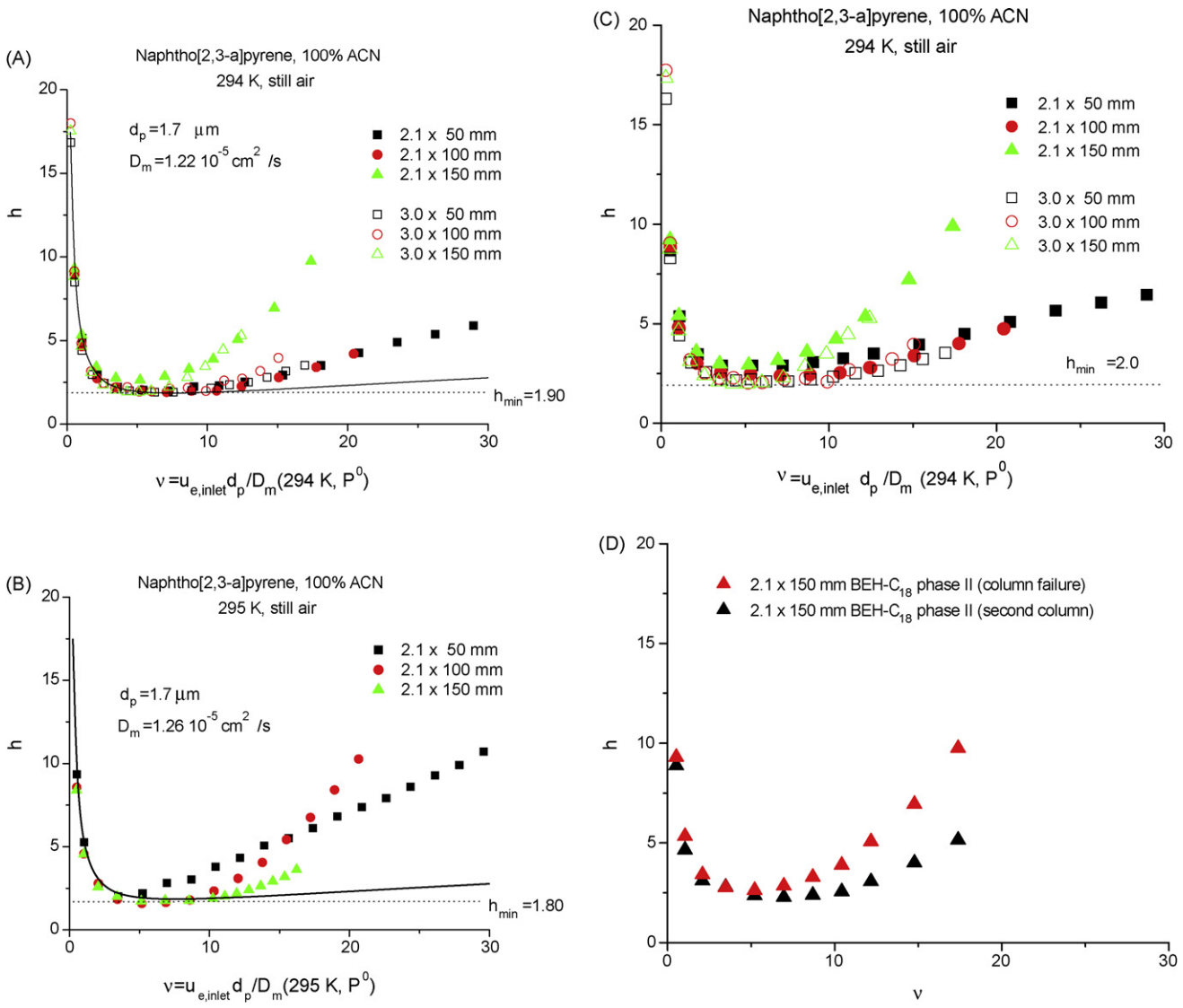

Fig. 3. (A) Comparison between the apparent reduced HETPs of six different prototype VHPLC columns as indicated in the legend of the upper graph. The columns were left free under still-air conditions. $T = 295$ K. Eluent: pure acetonitrile. The solid line represents the theoretical reduced HETP, in the absence of temperature gradients. (B) Same as in (A) except the first generation of VHPLC columns coming in 2.1 mm I.D., only. Note the improvement of the column performance for the shortest columns (50 and 100 mm). (C) Same as in (A) except the contributions of the extra-column volume to the column HETP were neglected. Note the better apparent performance of the large diameter columns. (D) The failure of a column is confirmed by the comparison of the reduced HETPs of the first and second 2.1 mm × 150 mm BEH-C_{18} prototype columns used.

generation of VHPLC columns. The B-term can be accurately measured from the data collected at 0.03 mL/min on the larger 3.0 mm I.D. columns. If we assume a parallel contribution of interparticle diffusion and particle diffusion to the overall column longitudinal diffusion, this reduced HETP term, h_{Long}, writes [23]:

$$h_{Long} = \frac{2\left(\gamma_e + \frac{1-\epsilon_e}{\epsilon_e}\Omega\right)}{\nu} \quad (5)$$

where $\gamma_e = 0.6$ is the external obstruction factor and Ω is the ratio of the particle diffusivity to the bulk diffusion term, considering the concentration gradient in the mesopores (e.g., in the bulk eluent phase) as the driving force for diffusion. From the experimental B-branch, the best value of Ω is 0.95. If surface diffusion were not participating to the effective particle diffusivity, Ω would be directly related to the diffusion along the mesopore and would be equal to the product of the particle porosity ($\epsilon_p = 0.43$), the internal obstruction factor, $\gamma_p = 0.6$, and the hindrance diffusion parameter, $F(\lambda_m)$ (equal to 0.65 for naphtho[2,3-a]pyrene) or $\Omega = 0.17$. Due to the significant retention of naphthopyrene ($k' = 2.20$), surface diffusion in the adsorbed state speeds up the effective sample diffusivity across the particles by a factor 5 to 6 a considerable effect. As a result, the mass transfer resistance due to diffusion through the porous particles is negligible and this reduced HETP term, h_{C_p}, writes [21]:

$$h_{C_p} = \frac{1}{30}\frac{\epsilon_e}{1-\epsilon_e}\left(\frac{\delta_0}{1+\delta_0}\right)^2 \frac{1}{\Omega}\nu \quad (6)$$

where δ_0 is given by:

$$\delta_0 = \frac{1-\epsilon_e}{\epsilon_e}\left[\epsilon_p + (1-\epsilon_p)K_a\right] \quad (7)$$

where K_a is the Henry's constant ($K_a = 4.43$). Hence, $\delta_0 = 5.03$ and $h_{C_p} = 0.0136\nu$. With $\nu < 30$, the contribution of h_{C_p} to h increases from 0 to only 0.40.

In contrast to their similarity at low flow rates, the behaviors of the second and first generations of VHPLC columns differ strongly at high flow rates. The performance of the shortest two columns of the second generation is much improved. Their C terms is clearly

lower than that of the first generation columns and the effects of heat friction seem considerably reduced. Yet, as will be shown later, the temperature profiles measured along the external surface of the tubes of the 2.1 mm I.D. prototype columns are very similar to those measured with the old Acquity BEH-C_{18} columns. Differences in the thermal heterogeneity of the packed beds do not suffice to explain the differences in the C terms. Since the trans-particle diffusivity is the same (identical B terms), this tends to suggest that either the external film mass transfer resistance was reduced by some modification of the external aspect of the particles or that the radial packing homogeneity has been improved, due to a change or an improvement in the packing process.

Surprisingly, an opposite behavior is observed with the longest column (150 mm). The minimum reduced HETP of this column is only 2.5 (instead of 1.9 for the columns of the older generation) and thermal effects seem to control the C-term of this column at high linear velocity, the experimental C-branch being strongly parabolic. This difference could be due to the failure of one single column during the manufacturing process. The combination of the heat effects and a trans-column flow heterogeneity could possibly explain this relatively poor column efficiency. Accordingly, we repeated the same experiments but with a second phase II 2.1 mm × 150 mm BEH-C_{18} column. Fig. 3D compares the reduced HETP of this new column to that of the first used column. This results confirms that the first column used did fail. The minimum reduced HETP of the second column is 2.0.

At this point, it would be hasty to propose a definitive explanation for the differences observed between the Van Deemter curves of the columns of the old and new generation. No information was yet released by the manufacturer regarding the preparation process nor the detailed properties of the new sub-2 μm prototype particles.

3.3. Effect of column geometry on the performance of the second generation of VHPLC columns

We first comment on the effect of the column length at constant inner diameter, then on the impact of the column tube diameter at constant length.

3.3.1. Column length L

As the column length increases, the maximum flow rate that the pump can deliver decreases from 1.90 mL/min to 1.45 mL/min and from 1.75 mL/min to 1.00 mL/min with the 3.0 and 2.1 mm I.D. columns, respectively. This explains why in Fig. 3A the reduced HETPs of the longest columns were not measured over the same range of reduced linear velocities as that of the shorter columns.

The effect of the column length is observed only at high flow velocities, when the temperature distributions along and across the packed bed are no longer uniform. Only a local HETP can be defined and the overall apparent column efficiency depends on the temperature distributions throughout the column in the steady-state eventually reached under the experimental thermal conditions, which are those of a column left in a still-air compartment. The column center becomes rapidly warmer than the wall region, except in the zone close to the column entrance due to the heat feedback along the very conductive stainless steel tube. The longer the column, the longer the distance over which the analyte band experiences a radial gradient of migration velocity, which results in a larger deviation of the experimental HETP curve from what is expected for an hypothetically isothermal column. The evidence of this thermal effect is shown in Fig. 3A by the parabolic shape of the C-branch of the 150 mm long columns. The same effect is moderate with the 100 mm long column and small with the 50 mm long columns. These effects are more pronounced with the large diameter columns (3.0 mm).

3.3.2. Column diameter d_c

It is interesting to compare the performance of VHPLC columns operated at the same superficial linear velocity and having the same length but different inner diameters, 2.1 and 3.0 mm. The flow rate ratio is nearly 2. Then, the pressure gradient, $(\Delta P/L)$ is the same along both columns and the frictional power P_f released per volume unit of packed bed is the same [5]:

$$P_f = u_S \frac{\Delta P}{L} \tag{8}$$

The amplitude of the radial temperature gradient, ΔT, is proportional to the frictional power liberated per unit of column length when the temperature of the wall is maintained constant or in the long-time limit conditions (infinitely long column) [6]:

$$\Delta T = \frac{1+\alpha_p T}{4\pi\lambda_p}\frac{F_v \Delta P}{L} \propto \frac{d_c^2}{d_p^2}\nu^2 \tag{9}$$

where α_p is the expansion coefficient of the eluent and λ_p is the effective thermal conductivity of the packed bed. At a constant reduced linear velocity ν, the temperature difference between the wall and the center of the column increases as the square of the column diameter. The additional reduced HETP term in the long-time limit due to the hydrodynamic contribution, h_{Aris}, writes [11]:

$$h_{Aris} = C_m \frac{\epsilon_e}{\epsilon_t(1+k')\Omega_r}\frac{d_c^2}{d_p^2}\nu \tag{10}$$

where C_m is the Aris contribution to the C-term [13,11], which depends on the radial profile of the analyte velocity across the column and Ω_r is the ratio of the radial dispersion coefficient to the bulk diffusion coefficient. The expression of C_m for small radial temperature amplitudes, ΔT, writes [11]:

$$C_m = \frac{1}{384}\left(B_\eta + \frac{k'_w}{1+k'_c}\frac{Q_{st}}{R}\right)^2\left(\frac{\Delta T}{T_w T_c}\right)^2 \tag{11}$$

where Q_{st} is the isosteric heat of adsorption, R the molar gas constant, k'_w and k'_c, and T_w and T_c are the retention factors of the analyte and the temperatures at the column wall and center, respectively.

Accordingly, if the long-time limit conditions are satisfied and the radial dispersion coefficient (Ω_r) is proportional to ν (dominant convective diffusion mechanism), the additional reduced HETP term, h_{Aris}, would approximately vary as:

$$h_{Aris} \propto \left(\frac{d_c}{d_p}\right)^6\left(\frac{\nu}{\bar{T}}\right)^4 \tag{12}$$

where $\bar{T}$ is the geometrical average of the temperatures T_w and T_c. Eq. (12) predicts that, at a fixed linear velocity, particle diameter and temperature, the additional HETP would increase as the sixth power of the column diameter. When the diameter of the column increases from 2.1 to 3.0 mm, h_{Aris} is expected to increase by a factor 8.5.

The experimental h *versus* ν data shown in Fig. 3A demonstrate, in fact, that the effect of the column diameter is not as dramatic as theoretically predicted in the range of linear velocities investigated in our experiments. Although the C-branches of the large diameter columns increase more rapidly than those of the small diameter columns, the difference in the h values of the two sets of columns is moderate. Increasing column diameters is not detrimental to the kinetic performance of VHPLC columns. This suggests that the long-time limit condition does not fully apply under the experimental conditions used in this study. This is confirmed by the results of our measurement of temperature profiles along column walls. Fig. 4 shows plots of the measured temperatures along the column wall as functions of the axial position along the column. The flow rates indicated correspond to the maximum flow rates applied during the

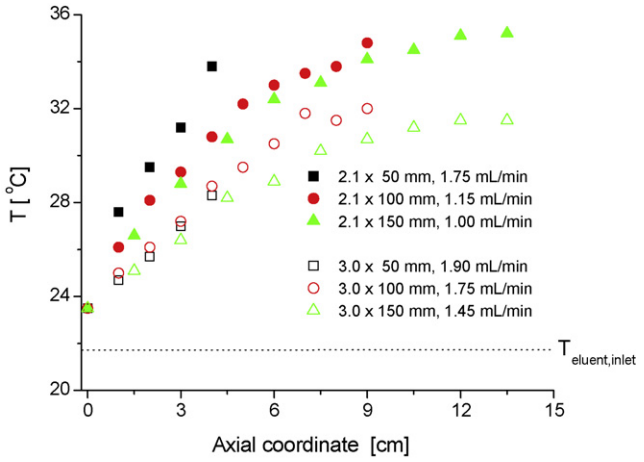

Fig. 4. Plots of the temperature of the external surface area of the six column tubes *versus* the axial coordinate *z*. The temperature of the eluent entering the column is 294.7 K. The columns are kept horizontal under still-air conditions, free from air convection. The flow rate and the column dimensions are given in the legend of the graph.

chromatographic runs of each column. The temperature profile has not yet reached its horizontal asymptotic limit for infinitely long columns [6]. The longer the column, the closer to this limit is the column wall temperature. Actually, the wall temperature increases significantly with increasing distance, *z*. The expression of ΔT given in Eq. (9) overestimates the true temperature difference between the center and the wall of all columns.

Nevertheless, it can be anticipated from the experimental HETP trends in Fig. 3A that the 3.0 mm I.D. columns would behave less well than the 2.1 mm I.D. columns at constant ν, for large flow rates. For $\nu < 13$, however, the two sets of columns behave very similarly.

For the common practitioner of chromatography, what matters the most is the observed peak resolution which includes the chromatograph's contributions to the band broadening. Wider and longer column should *a priori* be preferred provided the packing homogeneity is not affected by the dimension of the column tube during the packing slurry method. As the column volume increases, the band broadening taking place in the connecting tubes of the instrument becomes negligible in comparison to the band broadening caused by the sole mass transfer phenomena inside the packed column. Fig. 3C shows the corresponding reduced HETPs of the 2.1 and 3.0 mm I.D. VHPLC columns (phase II) which can be directly compared to those in Fig. 3A (extra-column contributions subtracted). It is obvious that the minimum reduced HETP is always better with the wider than with the thinner columns at a constant tube length. While the apparent minimum HETP is of the order of 2.5 particle diameters with the 2.1. mm I.D. columns, the apparent reduced HETP is close to 2.0 with the 3.0 mm I.D. columns. This is a substantial gain in band resolution and apparent column efficiency (295,000 *versus* 235,000 plates/m) provided the experimenter accepts to increase the consumption of the eluent's volume.

The extra-column volume of the VHPLC instrumentation is of the order of 15 μL. The hold-up volumes of the 2.1 and 3.0 mm × 50 mm columns are about 110 and 225 μL. In Fig. 3C, it is remarkable that the apparent minimum reduced HETP decreases from about 2.9 to about 2.1 upon increasing the column inner diameter. Accordingly, increasing the column diameter of small columns can strongly enhance their performance, especially when using instruments with large extra-column volumes. As suggested in a previous report [24], the extra-column volume should remain at least smaller than 5% of the column hold-up volume in order to avoid a significant loss in the column's performance.

Under isocratic conditions, narrowing down the column diameter limits the column performance to what the band broadening contribution of the equipment used permits. The injection system, the connecting tubes, and the detection cell should be examined in great details when performing separation with short narrow bore columns whose diameter is smaller than 1 mm, if one wishes to benefit from the excellent resolution power of sub-2 μm particles. The extra-column effects become much less relevant when gradients are used because the post-column volume is much smaller than the pre-column volume.

3.4. Temperature profiles along the second generation of VHPLC columns and models for their experimental C-term

The complete temperature profiles throughout the packed beds were calculated according to the procedure reported earlier [8], where all the necessary parameters can be found. It was assumed that the temperature of the eluent entering the column ($z = 0$) was 294 K. For all columns, the boundary condition along the column wall was the experimental temperature profile recorded along of this wall (Fig. 4), fitted to the following empirical relationship:

$$T_{\text{surface,wall}} = \frac{az}{1 + bz} \tag{13}$$

where *a* and *b* are two adjustable parameters.

The results of these calculations are shown in Fig. 5A–C (2.1 mm I.D. columns) and in Fig. 5D–F (3.0 mm I.D. columns). For each column, we used the maximum flow rate allowed by the pump (see values in Fig. 4). We compared the temperature difference between the column center and wall at the column outlet obtained from these calculations with that derived from Eq. (9) (the product $\alpha_p T$ is equal to −0.37 and $\lambda_p = 0.38$ W/m/K for acetonitrile). The results are given in Table 2. They clearly show that the columns are too short to reach the limiting ΔT values given by Eq. (9). The longer the column, the closer to this limit is the actual radial temperature gradient (−28% for the longest 15 cm long column). The discrepancy in the ΔT values arises from the fact that Eq. (9) assumes the temperature of the wall to be uniform, e.g., the column length should be infinitely long in practice [6].

3.4.1. Dispersion effects due to heat friction controlled by diffusion: Aris's model

Given the local temperature profile in Fig. 5A–F, it is possible to estimate the additional HETP term due to the radial gradient of the linear velocity of analyte migration across the column according to

Table 2
Calculated radial temperature amplitude ($T_c - T_w$) at the column outlet.

Column inner diameter (mm)	Column length (cm)	Flow rate (mL/min)	ΔT simulation (K)	ΔT limiting Eq. (9) (K)	Comparison (%)
2.1	5	1.75	2.98	4.97	−40
	10	1.15	1.38	1.92	−28
	15	1.00	1.02	1.41	−28
3.0	5	1.90	1.64	2.99	−45
	10	1.75	1.41	2.23	−37
	15	1.45	1.12	1.55	−28

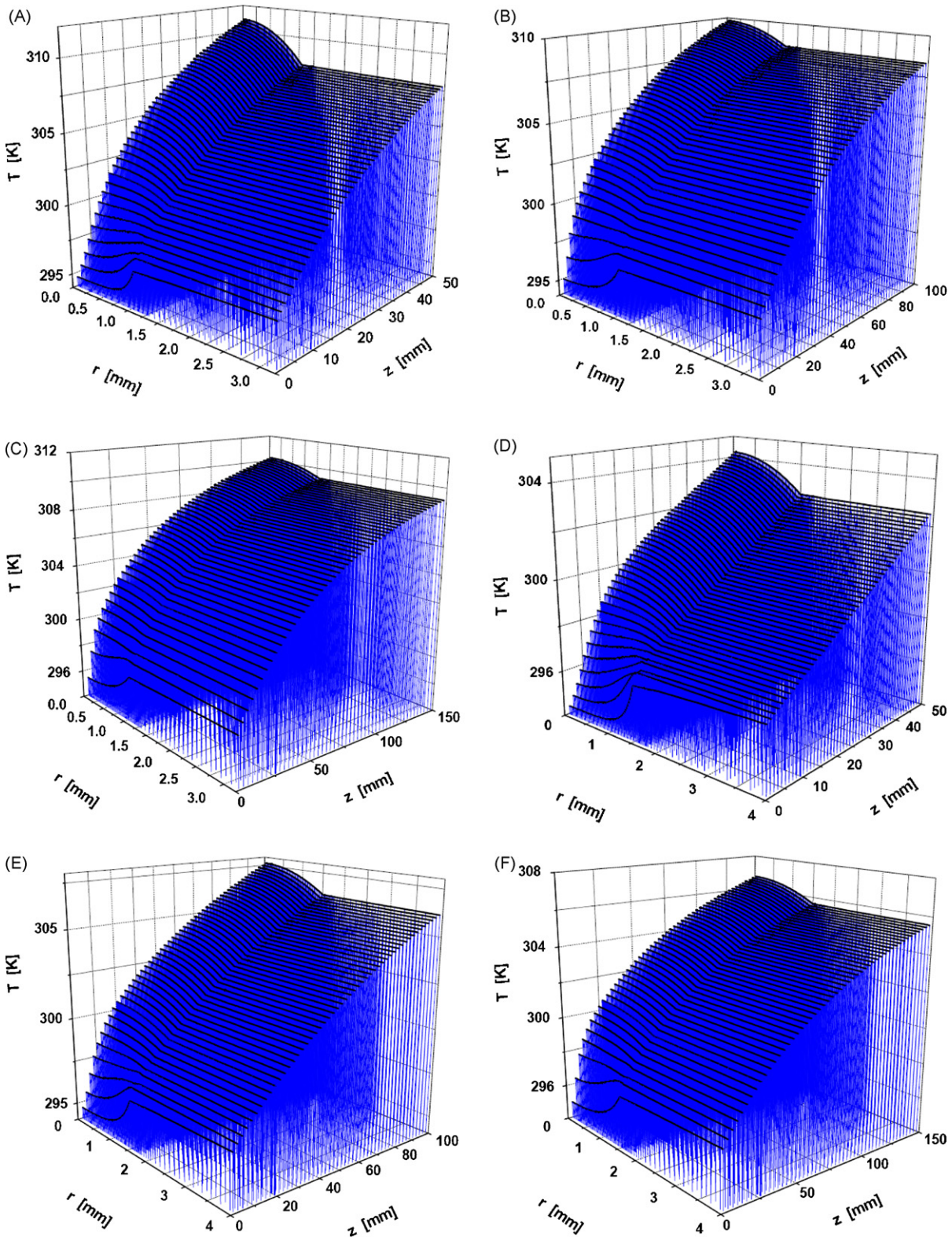

Fig. 5. Temperature distribution inside the six new prototype columns (packed bed + stainless steel tube) kept under still-air conditions at $T = 294$ K. The temperature of the eluent entering the column is 294 K. Same flow rates as those given in Fig. 4. Eluent: pure acetonitrile. (A) 2.1 mm × 50 mm column, (B) 2.1 mm × 100 mm column, (C) 2.1 mm × 150 mm column, (D) 3.0 mm × 50 mm column, (E) 3.0 mm × 50 mm column, and (F) 3.0 mm × 50 mm column.

the general dispersion theory of Aris [11]. The column was decomposed into 50 increments of equal length. For each one, the Aris coefficient C_m was calculated, the radial dispersion coefficient being taken from the results of NMR measurements made on packed columns [25]:

$$h_r = \frac{2\gamma_e}{\nu} + 0.32 \tag{14}$$

Table 3
Comparison between theoretical h_{Aris} terms and the deviation of the experimental HETPs from the isothermal reduced HETP.

Column inner diameter (mm)	Column length (cm)	Linear velocity (mm/s)	$\Delta h = h_{Diffusion}$ Aris model (Eq. (10))	$\Delta h = h_{Flow}$ flow model (Eq. (24))	Δh experiments (Fig. 3A)	$\Delta h_{Diffusion} - \Delta h_{exp.}$
2.1	5	3.4	28.2	2.8	3.6	+24.6
	10	2.2	4.5	1.6	2.0	+2.5
	15	1.9	2.6	1.5	2.9	−0.3
3.0	5	1.8	14.8	1.2	1.4	+13.4
	10	1.6	9.3	1.7	1.9	+7.4
	15	1.3	6.4	2.0	3.3	+3.1

$$D_r = \frac{h_r \epsilon_e \nu D_m}{2} = (\epsilon_e \gamma_e + 0.06\nu) D_m \quad (15)$$

The resulting $h_{Aris}(z)$ contribution was calculated according to Eq. (10) for each column segment. The overall additional reduced HETP term, $h_{Diffusion}$ for the whole column was simply derived from:

$$h_{diffusion,t} = \frac{1}{L}\int_0^L h_{Aris}(z)\,dz \quad (16)$$

There is a critical distance near the column entrance where the radial velocity profile is almost flat. Beyond that distance, the column center becomes increasingly warmer than its wall (see Fig. 5A–F). This critical distance is of the order of $(L/10)$ when the eluent entering the column is at the same temperature as the column compartment in which the column is kept horizontally under still-air condition.

The difference between the reduced HETPs measured and predicted for an ideal isothermal column was estimated by considering the difference between the experimental h data and the reference isothermal ($T = 294$ K) reduced HETP plot. This HETP model includes longitudinal diffusion, eddy dispersion, trans-particle diffusion and film diffusion as the four individual, independent mass transfer phenomena inside a column packed with spherical particles [26]:

$$h = \frac{2\left(\gamma_e + \frac{1-\epsilon_e}{\epsilon_e}\Omega\right)}{\nu} + \sum_{i=1}^{i=3} \frac{\omega_i \nu}{1 + \frac{\omega_i}{2\lambda_i}\nu} + \frac{1}{30}\frac{\epsilon_e}{1-\epsilon_e}\left(\frac{\delta_0}{1+\delta_0}\right)^2 \frac{1}{\Omega}\nu + \frac{2}{3.27}\frac{\epsilon_e^{5/3}}{1-\epsilon_e}\left(\frac{\delta_0}{1+\delta_0}\right)^2 \nu^{2/3} \quad (17)$$

The numerical values of the parameters of this reduced HETP equation were: $\gamma_e = 0.60$, $\epsilon_e = 0.38$, and $\delta_0 = 5.0$ at $T = 294$ K. The best values for the eddy dispersion parameters were: $\omega_1 = 0.01$, $\omega_2 = 0.24$, $\omega_3 = 2.00$, $\lambda_1 = 0.50$, $\lambda_2 = 0.23$, $\lambda_3 = 0.10$, directly taken from the guesses made by Giddings [27], including the trans-channel, short-range inter-channel, and long-range inter-channel flow inequalities, in order to generate a minimum reduced plate height of $h_{min} = 1.9$. The trans-column velocity bias effects were neglected. The best values of $\Omega = 0.95$ was obtained from the experimental B-branch of the experimental HETP curve at $T = 294$ K. Regarding the film mass transfer coefficient, we assumed that k_f was equal to half the value predicted by the Wilson and Geankoplis correlation [28], as recently observed experimentally for beds packed with porous particles [26,29]. This explains the scalar 2 in the numerator of the fourth term in the right-hand-side term of Eq. (17). The total isothermal reduced HETP curve is drawn in Fig. 2A and B for the sake of comparison with the experimental h data. It represents the minimum reduced HETP that can ever be measured.

Table 3 compares the additional reduced HETP caused by the heat effects, those predicted by the Aris model and those experimentally measured. It confirms that the longer the column and the residence time in the column, the better the agreement between experimental and theoretical results. With short columns, h_{Aris} overestimates the true band dispersion due to frictional heating because the analyte molecules cannot sample completely the column diameter. Actually, the Aris model is only valid for infinitely long residence time or infinitely long columns. Actual VHPLC columns are not operating under those strict conditions.

This suggests that the band dispersion is controlled and limited by another dispersion mechanism. Since there is not enough time for the analyte to sample the column diameter, the band broadening is controlled by a flow dispersion mechanism. This limiting mechanism would take place when no radial dispersion is allowed across the column or $D_r = 0$.

3.4.2. *Dispersion effects due to heat friction controlled by a flow mechanism: a flow model*

In this section, we assume that there is no sample dispersion, neither in the axial nor in the radial direction. Consider now a position z along the column where the radial temperature profile is correctly approximated by a parabolic function:

$$T(x,z) = T(0,z)(1 + \omega_z x^2) \quad (18)$$

The migration linear velocity $u(x,z)$ of the sample is then a function of the reduced radial position x because the retention factor k' depends on x *via* the change in temperature across the column diameter:

$$u(x,z) = \frac{\epsilon_e}{\epsilon_t}\frac{u_e(z,x)}{1 + k'(x,z)} \quad (19)$$

$u_e(x,z)$ depends also on the position (x,z) in the column because the viscosity and density of the eluent depend on the local temperature and pressure. The radial distribution of the mobile phase velocity due to the packing heterogeneity [30,31] is neglected. The heat effects are solely responsible for the trans-column velocity gradient; ϵ_e is assumed to be constant throughout the entire column. Because the radial temperature gradient is rather small (a few Kelvin or less), the Van't Hoff equation applies:

$$k'(x,z) = \frac{1-\epsilon_t}{\epsilon_t} K_0 \exp\left(-\frac{Q_{st}}{RT(x,z)}\right) \quad (20)$$

Accordingly, it takes a time $t(x)$ for the sample to migrate from the column inlet ($z = 0$) to its outlet ($z = L$) at the radial coordinate x:

$$t(x) = \int_0^L \mathrm{d}t(x,z) = \int_0^L \frac{\mathrm{d}z}{u(x,z)} \quad (21)$$

The analyte retention time (first moment) averaged across the column diameter is given by

$$\bar{t} = \mu_1 = 2\int_0^1 x t(x)\,\mathrm{d}x \quad (22)$$

The variance of the elution times $t(x)$ or second central moment is

$$\sigma_t^2 = \mu_2' = 2\int_0^1 x(t(x) - \bar{t})^2\,\mathrm{d}x \quad (23)$$

The additional reduced HETP $h_{flow,t}$ of the column caused by the radial heterogeneity of the flow distribution is then:

$$h_{flow,t} = \frac{L}{d_p}\frac{\sigma_t^2}{\bar{t}^2} \quad (24)$$

Table 3 lists the values of $h_{flow,t}$ derived using the calculated temperature profiles shown in Fig. 5A–D. The values of Q_{st} = 20.43 kJ/mol and $K_0 = 6.93 \times 10^{-4}$ were previously determined from the plot of the logarithm of the retention factor k' of naphtho[2,3-a]pyrene *versus* the reciprocal temperature in the temperature range [289–320 K] [12].

As it could have been anticipated, the values of $h_{flow,t}$ agree much better with the actual excess of HETP due to heat friction than those predicted using the dispersion model, controlled by a diffusion mechanism ($h_{diffusion,t}$). The calculated $h_{Flow,t}$ values are systematically smaller than the measured ones, which means that the actual contribution due to the flow heterogeneity is more important than that predicted by the mere existence of radial temperature gradients. We have neglected the possible trans-column flow heterogeneity which results from the irregularity of the packed bed due to the packing procedure. Our results demonstrate that the first 2.1 mm × 150 mm long column exhibits a more severely distorted flow profile than the other five columns, a result that is confirmed by its higher minimum reduced HETP of 2.5 (see Fig. 3A). The effects of frictional heat, (which make the central region of the column warmer than its wall region) and of the radial flow heterogeneity observed in packed columns (in which the flow velocity is smaller in the wall region than in the central region) add up to each other and could explain the poor performance of this thin (2.1 mm) and long (150 mm) new prototype column. This column failure was confirmed by the results of measurements of the reduced HETP data on a second 2.1 × 150 mm long column packed with the same material (Fig. 3D). Its minimum HETP is close to 2.0, the deviation from the isothermal HETP at high reduced velocity is considerably smaller and the agreement with theoretical values improved.

4. Conclusion

Our work illustrates the significant improvement in performance yielded by the 5 and 10 cm long new VHPLC columns, whether their inner diameter is 2.1 or 3.0 mm. Despite the fact that the heat power released on both sets of columns is the same, the C-branch of the new prototype columns deviates less from the one that would be observed in the absence of heat effects than do the C-branches of the first generation of VHPLC columns. For instance, at the high reduced linear velocity of $\nu = 30$, the number of theoretical plates of the 2.1 mm × 50 mm column increases from 4550 to 8350. At the more moderate reduced velocity of $\nu = 20$, the number of theoretical plates of the 2.1 mm × 100 mm column increases from 9500 to 25,000. These are very important gains. On the other hand, a significant deterioration of the column performance was observed for the longest columns (150 mm). At $\nu = 16$, the number of theoretical plates of the 2.1 mm × 150 mm column decreases from 40,050 to 15,000. This difference could be attributed to a single column failure during the whole manufacturing process. The data should be repeated on a new column.

The analysis of the increase in the reduced HETP that is caused by the heat effects demonstrates that this extra band broadening is in part caused by the radial heterogeneity of the flow velocity due to the radial temperature gradient. The diffusion controlled mechanism of band dispersion derived from the general dispersion theory of Aris [11] applied to packed LC columns overestimates the actual amount of band broadening in the shortest two columns. The comparison between the experimental h data and the h values predicted by a simple flow dispersion mechanism suggests that the radial profile of mobile phase velocities under isothermal conditions is not flat. It contributes to a slight increase of the reduced HETP of the shortest columns (+0.4 to 0.8 and + 0.2 for the 2.1 and 3.0 mm I.D. 5 cm long columns, respectively) and it seriously impair the column performance of the longest and thinnest column (+ 3 h unit with the 2.1 mm × 150 mm column). The mechanism of dispersion in VHPLC columns is definitely based on a flow mechanism.

In conclusion, the new VHPLC prototype adsorbent packs very well in short columns. It provides short columns having an excellent efficiency. In contrast, it seems to be difficult to pack it into long columns, particularly in those using thin diameter tubes. Lacking information regarding this new material and how it differs from the one previously used, we cannot suggest any explanation for these observations.

Finally, our work demonstrates than the radial distribution of the column porosity, hence permeability and velocity, plays an important role in controlling the eventual efficiency of short VHPLC columns. The dispersion model that is controlled by a flow mechanism and neglects diffusion of the analyte across the column diameter provides better predictions of the C-branch behavior of short VHPLC columns, which are run very rapidly with retention times smaller than a minute, leaving insufficient time for the analyte to sample properly the whole velocity distribution across column diameters of 3.0 mm or even 2.1 mm. The question remains whether and under which conditions heat effects or radial column heterogeneity influences most the *C*-term of VHPLC columns. Trans-column flow heterogeneity can be measured either by using local electrochemical detection at different radial positions across the column exit or by measuring the reduced HETPs of the column at high linear velocities when the mesopores are blocked under conditions where heat effects are negligible. These investigations are in progress and their results will be reported later.

Nomenclature

a	Empirical coefficient in Eq. (13) (K m^{-1})
b	Empirical coefficient in Eq. (13) (K m^{-1})
A_η	Parameter in Eq. (3)
B_η	Parameter in Eq. (3)
C_m	Aris coefficient
d_c	Column diameter (m)
D_r	Radial dispersion coefficient (m^2/s)
D_h	Hydrodynamic diameter (m)
D_m	Bulk diffusion coefficient (m^2/s)
d_p	Average particle size (m)
F_v	Flow rate (m^3/s)
H	Axial column HETP (m)
$H(z)$	Axial column HETP at coordinate z (m)
h_{Aris}	Additional axial column reduced HETP term given by the Aris' general theory of dispersion
h	Axial reduced column HETP
h_{C_p}	reduced intra-particle mass transfer resistance HETP term
$h_{diffusion,t}$	Overall additional Aris reduced column HETP
$h_{flow,t}$	Overall additional flow reduced column HETP
h_{Long}	Reduced longitudinal diffusion HETP term
h_r	Radial reduced column HETP
k'	Retention factor
k'_c	Retention factor at the center of the column
k'_w	Retention factor at the wall of the column
$k'(z,x)$	Local retention factor
k_0	Column specific permeability
K_a	Henry's constant
K_c	Kozeny-Carman constant of the packed bed
L	Column length (m)
P_f	Power heat friction (W m^{-3})

P Pressure (Pa)
Q_{st} Isosteric heat of adsorption (kJ/mol)
r Radial column coordinate (m)
R Molar gas constant (J/mol/K)
R_c Column inner diameter (m)
T Temperature (K)
T_c Temperature at the column center (K)
T_w Temperature at the column wall (K)
$T_{surface,wall}$ Temperature at the column wall (K)
$\bar{T}$ Geometric average temperature defined in Eq. (12) (K)
$T(x,z)$ Local temperature (K)
t_R Retention time recorded in presence of the column at the apex of the peak (s)
t_e Retention time recorded in absence of the column at the apex of the peak (s)
$t^r_{1/2}$ Elution of the rear desorption part of the band profile recorded in presence of the column at half the height of the peak (s)
$t^f_{1/2}$ Elution of the front adsorption part of the band profile recorded in presence of the column at half the height of the peak (s)
$t^r_{1/2,e}$ Elution of the rear desorption part of the band profile recorded in absence of the column at half the height of the peak (s)
$t^f_{1/2,e}$ Elution of the front adsorption part of the band profile recorded in absence of the column at half the height of the peak (s)
$t(x)$ Elution time at the radial coordinate x (s)
$t(x,z)$ Local elution time (s)
$\bar{t}$ Column cross-section average elution time (s)
u_S Superficial chromatographic linear velocity (m/s)
$u(z,x)$ Local linear velocity of the elute (m/s)
$u_{e,inlet}$ Interstitial linear velocity (m/s)
$u_e(z,x)$ Local superficial linear velocity (m/s)
x Reduced radial coordinate r/R
z Longitudinal column coordinate (m)

Greek letters
α_p Average expansion coefficient of the eluent (K^{-1})
δ_0 parameter defined in Eq. (7)
ΔT Temperature amplitude (K)
ΔP Pressure drop over the column length (Pa)
ϵ_e External porosity of the packed bed
ϵ_p Porosity of the particles
ϵ_t Total porosity of the column
η_S Viscosity of the eluent (Pa s)
μ_1 First moment of the elution times $t(x)$ (s)
μ'_2 Second central moment of the elution times $t(x)$ (s^2)
γ_e Obstruction factor of the packed bed
λ_i Giddings's flow parameter in the eddy dispersion term in Eq. (17)
λ_p Heat conductivity of the packed bed immersed in the eluent (W/m/K)
ν Reduced interstitial linear velocity calculated at the column inlet
ω_i Giddings's diffusion parameter in the eddy dispersion term in Eq. (17)
ω_z Relative temperature difference between the center and the wall of the column
Ω Relative sample diffusivity (particle to bulk)
Ω_r Relative sample diffusivity across the column (column to bulk)
σ^2_t Variance of the elution times $t(x)$ (s^2)
ζ parameter defined in Eq. (3) (Pa^{-1})

Acknowledgements

This work was supported in part by grant CHE-06-08659 of the National Science Foundation and by the cooperative agreement between the University of Tennessee and the Oak Ridge National Laboratory. We thank Uwe Neue (Waters, Milford, USA) for the generous gift of the columns used in this work and for fruitful discussions.

References

[1] 32nd International Symposium on High Performance Liquid Phase Separations and Related Techniques. Baltimore, MD, May 10–16, 2008.
[2] T. Chester, Am. Lab. 41 (2009) 11.
[3] P. Bristow, J. Knox, Chromatographia 10 (1977) 279.
[4] G. Guiochon, J. Chromatogr. A 1168 (2007) 101.
[5] H. Lin, S. Horváth, Chem. Eng. Sci. 36 (1981) 47.
[6] H. Poppe, J. Kraak, J. Huber, H. van der Berg, Chromatographia 36 (1981) 515.
[7] F. Gritti, G. Guiochon, Anal. Chem. 80 (2008) 6488.
[8] F. Gritti, G. Guiochon, Anal. Chem. 80 (2008) 5009.
[9] U. Neue, M. Kele, J. Chromatogr. A 1149 (2007) 236.
[10] F. Gritti, G. Guiochon, J. Chromatogr. A 1187 (2008) 165.
[11] F. Gritti, M. Martin, G. Guiochon, Anal. Chem. 81 (2009) 3365.
[12] F. Gritti, G. Guiochon, J. Chromatogr. A 1206 (2008) 113.
[13] R. Aris, Proc. Roy. Soc. A 235 (1956) 67.
[14] M. Martin, G. Guiochon, Anal. Chem. 54 (1982) 1533.
[15] F. Gritti, G. Guiochon, J. Chromatogr. A 1216 (2009) 1353.
[16] R. Plumb, J. Mazzeo, E. Grumbach, P. Rainville, M. Jones, T. Wheat, U.D. Neue, B. Smith, K. Johnson, J. Sep. Sci. 30 (2007) 1158.
[17] Pittcon Conference & Expo 2009. Chicago, IL, March 8–13, 2009.
[18] F. Gritti, G. Guiochon, J. Chromatogr. A 1169 (2007) 125.
[19] F. Gritti, G. Guiochon, J. Chromatogr. A 1138 (2007) 141.
[20] I. Rustamov, T. Farkas, F. Ahmed, F. Chan, R. LoBrutto, H. McNair, Y. Kazakevich, J. Chromatogr. A 913 (2001) 49.
[21] G. Guiochon, A. Felinger, A. Katti, D. Shirazi, Fundamentals of Preparative and Nonlinear Chromatography, 2nd ed., Academic Press, Boston, MA, 2006.
[22] C. Wilke, P. Chang, AIChE J. 1 (1955) 264–270.
[23] F. Gritti, G. Guiochon, Anal. Chem. 78 (2006) 5329.
[24] F. Gritti, A. Felinger, G. Guiochon, J. Chromatogr. A 1136 (2006) 57.
[25] U. Tallarek, D. van Dusschoten, H. Van As, E. Bayer, G. Guiochon, J. Phys. Chem. B 102 (1998) 3486.
[26] F. Gritti, G. Guiochon, AIChE. J., AICHE-09-11844, in press.
[27] J. Giddings, Dynamics of Chromatography, Marcel Dekker, New York, NY, 1965.
[28] E. Wilson, C. Geankoplis, J. Ind. Eng. Chem. (Fundam.) 5 (1966) 9.
[29] F. Gritti, G. Guiochon, AIChE. J., AIChE-09-11930, in press.
[30] T. Farkas, G. Guiochon, Anal. Chem. 69 (1997) 4592.
[31] J. Abia, K. Mriziq, G. Guiochon, J. Chromatogr. A 1216 (2009) 3185.